STScI | SPACE TELESCOPE SCIENCE INSTITUTE

JWST TECHNICAL REPORT

Title: Detection and Flagging of Showers and Snowballs in JWST	Doc #: JWST-STScI-008545, SM-12 Date: 3 June 2024 Rev: A
Authors: Michael Regan Phone: 410 - 338 - 4769	Release Date: 21 June 2024

1 Abstract

The radiation environment at L2 yields a large number of cosmic rays that affect JWST detectors. The vast majority of these events deposit charge in only one or two pixels, and the baseline JWST pipeline has a jump step that flags these events to prevent them from affecting the flux determination. In addition, there is a different population of large radiation events that affect both the NIR and MIRI detectors. These large events ("snowballs" in the NIR and "showers" in MIRI) contain regions that are not flagged by the baseline jump step. Left undetected, these large events strongly affect deep exposures.

In this report I describe both the characteristics of snowballs and showers and the algorithms for detecting the affected regions. In addition, I explain how the various step parameters affect the detection of Snowballs and Showers.

2 Large Cosmic Ray Events: Snowballs and Showers

Early in JWST commissioning, one unexpected detector effect we observed was large cosmic ray events. While a classic cosmic ray affects only one or two pixels (except for ones with high angles of incidence), these large events affected up to hundreds of pixels. In general, these large events also generated low level diffuse emission, and some of the affected pixels showed elevated count rates for the rest of the integration or longer. While the baseline pipeline jump detection algorithm is able to flag the large instantaneous jumps within these large events, it is unable to flag both the diffuse and long-term components.

The large events in the near infrared H2RG detectors were seen in ground testing of the Hubble WFC3 Near IR (Hilbert 2009, McCollough 2009) and in the JWST NIRSpec (Rauscher et al 2014) and NIRCAM, but the rate and variations in morphology were higher on-orbit. In the ground-based testing, the events were uniformly circular which led to them being called snowballs. The event rate was around 1 x 10^{-4} events per million pixels per second and the radius was 5-10 pixels. Because this low rate decreased with time, the expectation was that during on-orbit they would be insignificant. However, what we see on-orbit are events that are several orders of magnitude more frequent and with sizes that range from 10 to greater than 1000 pixels.

In contrast, the large events we see in the MIRI detectors were first seen on-orbit. A large fraction of these events are tight clusters of excess classic cosmic rays centered on a region of diffuse emission. This led to them being named showers. They have a similar frequency to the snowballs but affect the detectors in a significantly different manner.

In this report, I will discuss the characteristics of these snowballs and showers. Then, for each type of event, I will detail the new JWST pipeline algorithm that is used to flag the affected samples to remove the effects of the snowballs and showers. I will also explain the various parameters that control the algorithm and how these parameters affect the sensitivity and specificity of the detection process.

3 Near Infrared Snowballs

In Figures 1 - 3, I show examples of the residual effects of snowballs on rate images seen in dark exposures for each of the JWST near infrared detectors. The residual snowballs actually look like doughnuts in the rate images because the center of the snowball is saturated which causes the pipeline to ignore all samples in those pixels after arrival of the snowball. Meanwhile, the outer regions are below the detection threshold and don't get flagged. In addition, for the larger snowballs, there can be a smaller inner ring that appears inside of the diffuse halo. In the next section I will breakdown the components of the snowballs. The mapping of the full raw uncalibrated data to the short name is in Table 1

Table 1 - Raw uncalibrated files mentioned in the Near Infrared

Exposure File Name	Label
jw01062099001_02101_00001_nrca1_uncal.fits	N0
jw01497005001_02201_00001_nis_uncal.fits	N1
jw01121002001_02102_00002_nrs2_uncal.fits	N2
jw01121002001_02102_00003_nrs1_uncal.fits	N3
jw02123001001_02101_00001_nrs1_rate.fits	N4

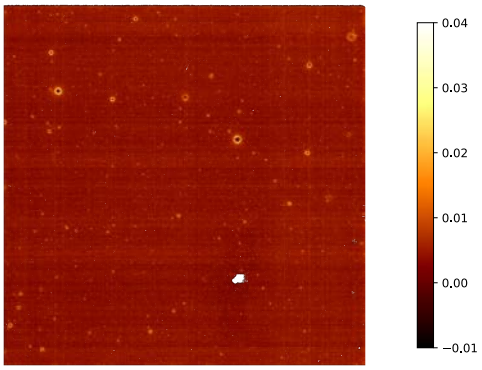

Figure 1 – A NIRCAM dark rate image (DN/s) showing the residuals of snowballs. This is a 140-frame integration taken in rapid mode which is a total exposure time of 1500 seconds. It has a snowball rate of 0.25 events per million pixels per second. (exposure N0)

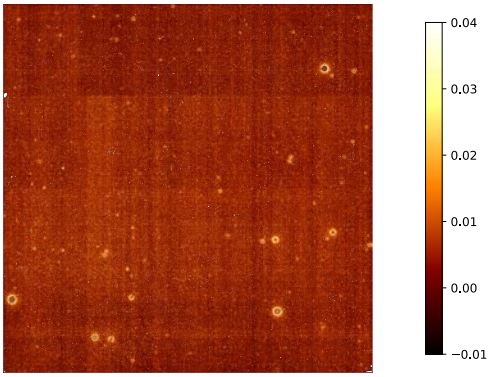

Figure 2 - A NIRISS dark rate image (DN/s) showing the residuals of snowballs. This is a 120-frame integration taken in rapid mode which gives a total exposure time of 1300 seconds. It has a snowball rate of 0.48 events per million pixels per second. (exposure N1)

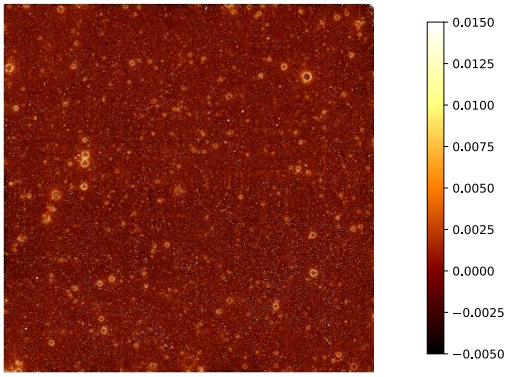

Figure 3 A NIRSpec dark rate image (DN/s) showing the residuals of snowballs. This is a 245-frame integration taken in rapid mode which gives a total exposure time of 3600 seconds. It has a detected snowball rate of 2.3 events per million pixels per second.The longer integration time causes the snowballs to be more prominent than in the NIRCAM and NIRISS images. The first reason is that the longer time lowers the uncertainty in the rate fit. The second is that the total number of snowballs is increased proportionally to the integration time. (from N2)

3.1 Snowball Morphology

The baseline cosmic ray detection step in the JWST pipeline is the jump step. This step works with the differences between adjacent groups in an integration to find differences that are above a statistical threshold for each pixel. The threshold is determined using the read noise and gain reference files to find the expected noise for each difference.

In Figure 4, I show a series of the difference images starting with the group where the snowball occurred. In the first frame, we can see there is a large jump in the center of the snowball (the core is always saturated in snowballs) surrounded by an extended halo where the charge is falling off exponentially with increasing radius until it is lost in the read noise. The second frame shows the now saturated core with no net signal surrounded by a ring with significant charge. This ring extends into the third frame and shows a positive signal for the rest of the integration. This signal is due to charge migration from the saturated core.

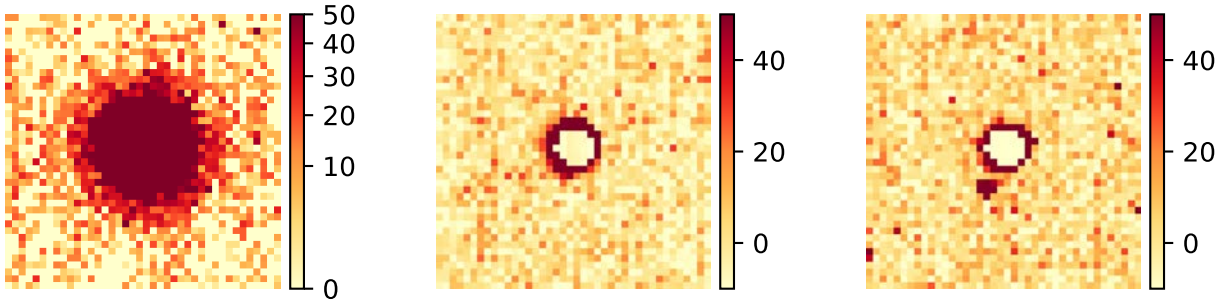

Figure 4 – A set of the sequential difference images starting with the left panel. The initial snowball is shown in the left panel. The snowball shows an exponential decay in the accumulated charge from the center. This is what causes the diffuse halo in the rate image. The differences in the outer region are below the threshold of classic jump detection (~25 DN for this example). The center panel is the first group after the snowball, while the right panel shows the second group after the snowball. The second and third panels show that the inner ring surrounds the saturated core. This is caused by charge migration from the super saturated core. (from N3)

In Figure 5, I show the Data Quality (DQ) output from the baseline jump detection code for the snowball in Figure 4. Pixels that have a DQ value of 4 (Jump) leading to a break in the ramp fit, causing the ramp fitting process to solve for separate rates and then combine them for a rate estimate. Pixels that have a DQ value of 2 (Saturation) cause all subsequent samples to be ignored for the ramp fit. Here you can see that the core is flagged as saturated for all frames. In the initial frame, the core is enclosed by a ring of pixels that are flagged as Jump by the baseline algorithm. One of the causes of the snowball residuals in the rate images is apparent when we compare the radius of extra halo emission in the difference image (Figure 4) to the radius of the pixels flagged as Saturated or Jump (Figure 5). The baseline jump flagging does not cover the entire halo. These unflagged halo pixels cause the outer region of excess emission shown in Figures, Figure 1-Figure 3. Also, we can see in the last panel of Figure 5 that the saturated core is no longer surrounded by a region that is flagged as Jump. This is because the charge spilling out of the saturated core is below the baseline jump detection threshold. This leads to the charge spilling ring we see around the center of snowballs in Figures, Figure 1-Figure 3.

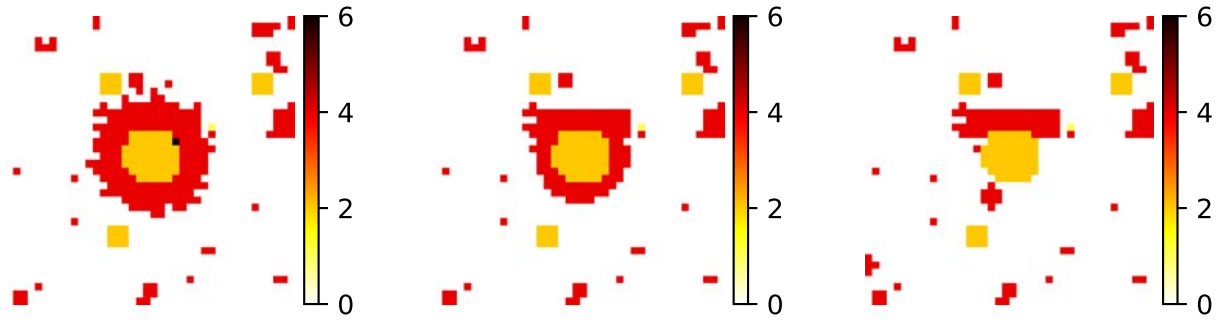

Figure 5 – Data Quality (DQ) extension for the snowball in Figure 4. This figure shows output from the saturation and classic jump detection steps of the pipeline. The DQ values of interest are 2 (Saturation) and 4 (Jump). The yellow pixels are the ones that have been flagged as Saturation, while red indicates the pixels that have been flagged as Jump. Notice how the jump region around the saturated core does not extend as far as the snowball in the left panel of Figure 4. (from N3)

The lack of flagging neither the pixels in the charge spilling ring nor the pixels with diffuse emission out to large radii is why we need an additional algorithm for exposures affected by snowballs.

3.2 The Snowball Detection Algorithm (performed after the baseline jump detection algorithm)

The snowball detection algorithm needs to flag the two regions within snowballs that are not flagged in the baseline jump algorithm: the charge spilling ring and the faint extended halo.

3.3 Snowball Algorithm Steps (repeated for every group)

1. Find all the newly saturated pixels. Because snowballs always have a saturated core, we require that there are saturated pixels in the center of the snowball.
2. For all sets of connected saturated pixels that are above the minimum required area (**min_sat_area**), solve for the parameters of the minimum enclosing ellipse.
3. Find all the newly flagged jump pixels. For all sets of connected jump pixels that are above the minimum required area parameter (**min_jump_area**), solve for the parameters of the minimum enclosing ellipse.
4. For each jump ellipse that has a newly saturated pixel at the center of the ellipse, add the jump ellipse parameters to the list of snowballs. The requirement that snowballs have a newly saturated central pixel is removed for jump ellipses closer than the **edge_size** parameter from the edge of the detector. This is to allow snowballs that impact on the reference pixels to be flagged. This does lead to more false positives near the edges.
5. For each saturated ellipse, if the minor axis of the saturated ellipse is larger than the minimum radius parameter (**min_sat_extend**), extend the region of saturation by the number of pixels expansion value parameter (**sat_expand**). This extended region is flagged as saturated for the remainder of the integration. This will flag the charge spilling ring.
6. For each jump ellipse, expand the minor axis by multiplying the minor axis by the jump expand parameter (**expand_factor**), then expand the major axis by the same number of pixels as the minor axis. Expanding the major axis by the number of pixels in the minor axis is a better match to the diffuse halo than keeping the same axis ratio. This will flag the charge spilling ring.
7. All expansions are limited by a parameter (**max_extended_radius**). This is currently set to 200 pixels by default to prevent any pathological observations from flagging all the pixels and crashing the production pipeline.

In Figure 6, I show the updated DQ flagging of the snowball shown in Figures 4 and 5. The significantly larger radius of pixels being flagged as Jump in Figure 7 does cover the excess counts in the diffuse halo that we see in the difference image. The expanded saturated core now encompasses the charge spilling ring.

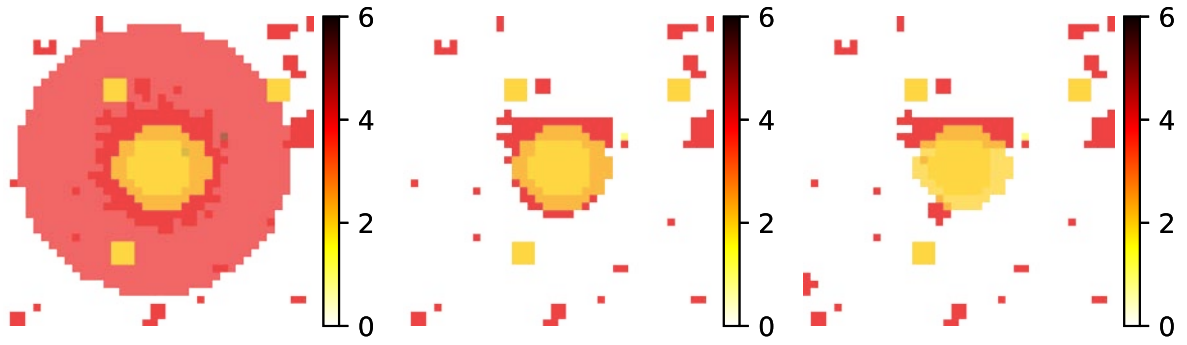

Figure 6 – An overlay of the of the original flagging and the updated snowball algorithm flagging initial pixels on the left panel and then the next two groups. The darker yellow region is the original saturation flagging, and the darker red is the original jump flagging. In the left panel, we can see that the saturated core has been expanded to be larger than in Figure 5. This larger saturated core suppresses the charge spilling ring. We can also see that the expanded jump region encompasses the diffuse halo. The snowball flagging only affects the second and third groups by the increase in the radius of the saturated core. (from N3)

3.4 Results of the Snowball flagging algorithm

In Figure 7 -Figure 9, I show the before and after rate images for sample dark exposures for each of the near infrared instruments. The results show that almost all of the snowball effects have been removed.

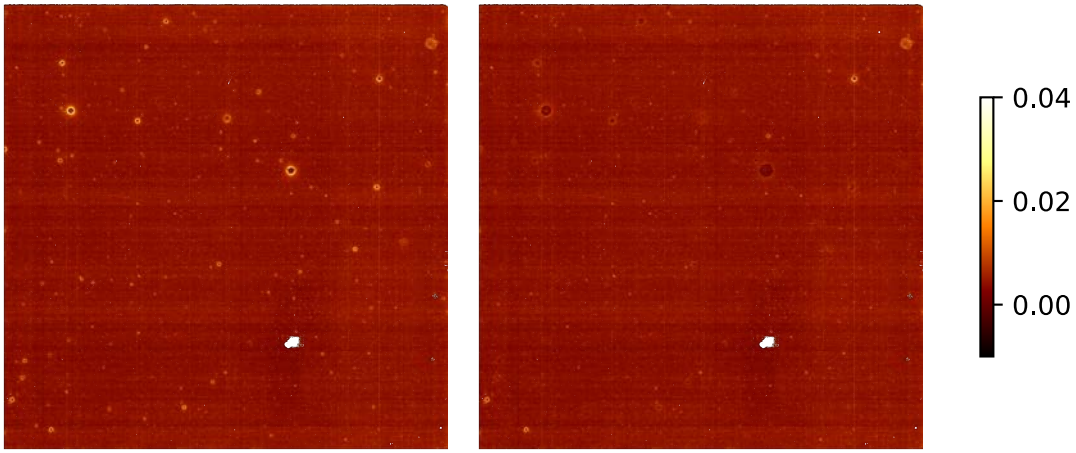

Figure 7 – (left) The NIRCAM dark rate image shown in Figure 1. This is a 140-frame integration taken in rapid mode which is a total exposure time of 1400 seconds. It has a snowball rate of 0.25 events per million pixels per second. (right) The resulting rate image after the snowball algorithm has been applied. While a couple of breakthrough snowballs are visible, the majority have been removed. (from N1)

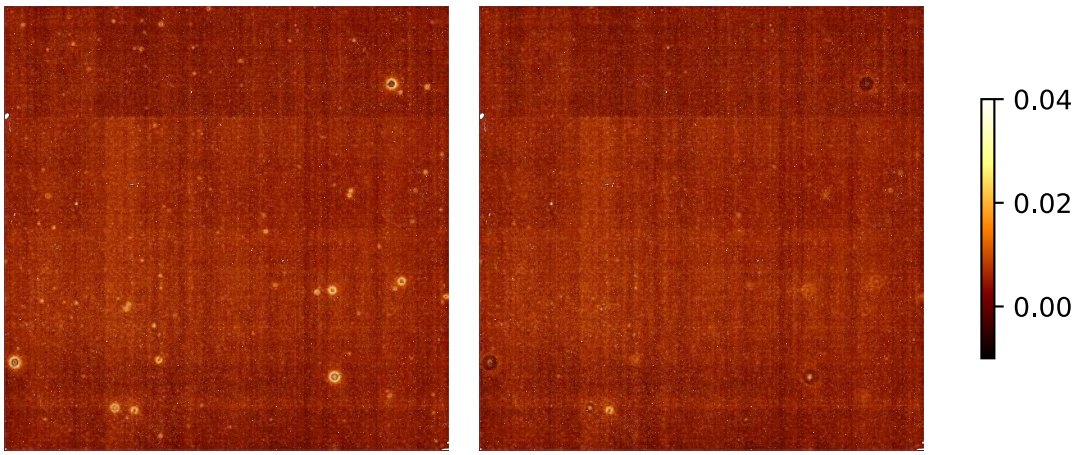

Figure 8 – (left) The NIRISS dark rate shown in Figure 2. (right) The resulting rate image after the snowball algorithm has been applied. Only one snowball is unflagged. (from N2)

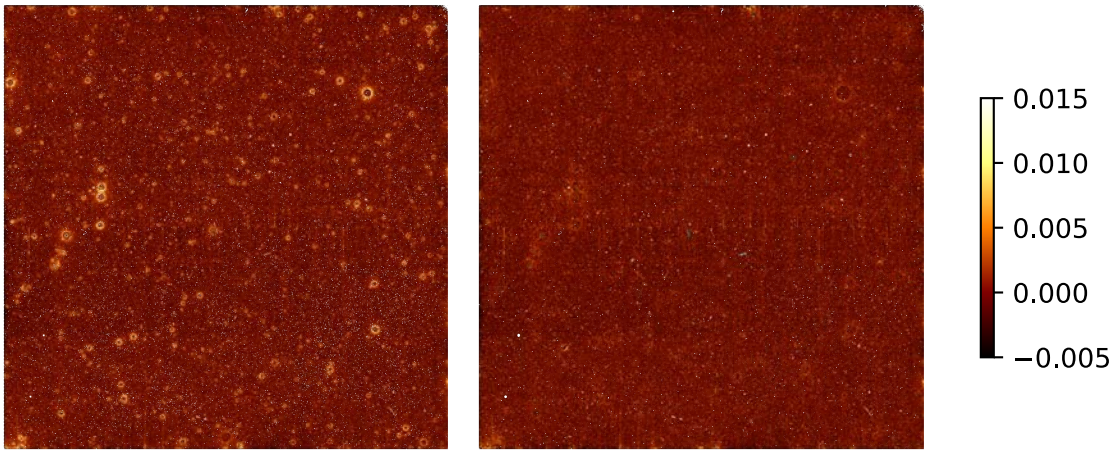

Figure 9 – (left) The NIRSpec rate image shown in Figure 3. (Right) The corrected rate image. Here the major residual is the snowball whose saturated center is on the reference pixels. Otherwise, there are relatively few unflagged snowballs given the initial quantity. (From N3)

3.5 Grouped Frames and Snowballs

To reduce the data volume generated by the readout of JWST detectors, the onboard hardware can average or drop frames to create groups. This averaging affects the baseline snowball algorithm. For example, the baseline NIRSpec readout pattern averages every four frames to form a group. This averaging means that if a snowball occurs between any two frames within the group, the saturated core will not get flagged as saturated in the group where it actually occurred (Note that there are plans to flag the correct group.) Instead, it will not get flagged as saturated until the group after the snowball. Alternatively, if the snowball was to arrive between two groups, then the algorithm would work the same as if the frames were not averaged into a group. In Figure 10, I show two planes of the DQ flags when a shower occurs within a group. The lack of saturation in the first group would cause it to not be detected as a snowball. The second group would nominally get detected.

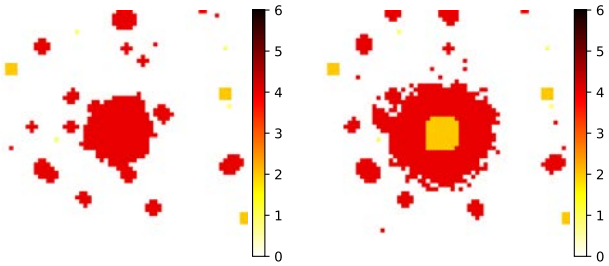

Figure 10 - (left) The DQ flag of an averaged group where the snowball has occurred. It is not saturated in the core because the average values are below the saturation threshold. (right) The snowball DQ flags in the group after the arrival. Here it looks like a normal snowball, but the rough boundary of the edges of the jump region shows that it was not detected as a snowball. (from N4)

To correctly flag the diffuse emission in the non-saturated group, the algorithm checks to see if in the next group there is new saturation in the center. If this is true, then the first group only expands the jump ellipse. The second group gets both the expansion of the saturated core and the jump ellipse (Figure 11).

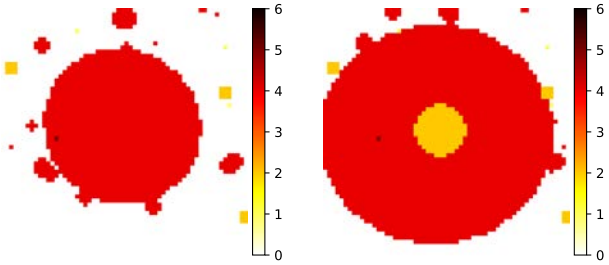

Figure 11 - (left) The DQ flag in the group where the actual snowball occurred after the snowball flagging algorithm has run. (right) The DQ flags for the group after the snowball where the algorithm has correctly identified the snowball.

3.6 Outstanding issues with Snowball detection

- The option of not requiring saturated cores on the edges of the detector can lead to some false positive snowball detections. This can be greatly reduced by increasing the minimum jump area for a snowball to be detected, but that yields undetected small snowballs over the entire detector. A separate minimum size parameter for the edge of the detector would a better solution.
- Bright stars that saturate the core of their point spread function early in the integration can be flagged as a snowball. While this is incorrect, it is not clear what the consequences are.
- The optimum number of pixels to expand the saturated core depends on the size of the saturated core. Having a single value requires either over expanding small snowballs or under expanding large snowballs.

3.7 Jump Step Parameters that control the Snowball Detection and Flagging

The following is a list of the parameters that affect snowball detection and a short description of what the parameter controls. For each parameter the value in parentheses is the default value in the code. This can be overridden by either a parameter reference file or a command line parameter.

- expand_large_events- This is the Boolean value that determines if the snowball flagging algorithm will be used. It should always be set to False for MIRI observations. (True for NIR instruments)
- find_showers –This should only be set to False for all NIR observations. (False)
- min_sat_area – The minimum number of contiguous pixels flagged as saturated for the algorithm to detect saturation as the center of the jump. Increasing this area will lead to less flagging of small events. Note that this parameter is not relevant in the region within the edge size. (1.0)
- edge_size – Pixels within this distance from the edge of the detector skip the requirement for snowballs to have a saturated pixel at the center of the jump ellipse. This is to allow snowball flagging for events that occur on the reference pixels which do not saturate. (25)
- min_jump_area – The minimum number of contiguous pixels flagged as Jump for the algorithm to create a jump ellipse. Increasing this will lead to less flagging of small events. (5.0)
- expand_factor – The expansion factor that will be multiplied by the minor axis of the jump ellipse to make it larger. This extends the jump flagging into the diffuse halo region of extended emission. The major axis is not multiplied by expand_factor. It is extended by the same number of pixels as the minor axis. Otherwise, highly elliptical snowballs would flag too many pixels. (2.0)
- sat_required_snowball – If True, then the center of the jump ellipse must have a saturated pixel. The default value is True. Setting it to False will increase the number of false positive detections but can be a workaround for grouped readout patterns until the changes described in section 3.5 are in production. If set to False, **min_jump_area** should be increased. (True)
- min_sat_radius_extend – The minimum radius of the saturated core of the snowball for the region of saturation to be extended. In general, because the pipeline saturation flagging of small snowballs already extends out by a pixel, small saturated cores do not need to be extended. (2.5)
- sat_expand – The number of pixels to extend the diameter of saturation flagging for the saturated cores of snowballs. This is to flag the charge spilling ring around the saturated core. (2)
- max_extended_radius - This is set to 200 pixels to prevent rare outlier values from flagging all the pixels and crashing the production pipeline. If a large snowball seems to have the core correctly flagged, but there is a residual ring of halo emission, changing this parameter to a much larger number (> 500) can improve the results. (200)

4 MIRI Showers

4.1 Shower Morphology

In general, there is a larger spread in morphology for showers compared to snowballs. The diversity of morphologies implies that the underlying causes of the two large events may be different. The various examples of MIRI showers were selected from a set of darks taken in the fall of 2022. Table 2 lists the full file name and the label used for that exposure.

Table 2 - MIRI raw data files and the label used in the text.

Exposure File Name	Label
jw01517157001_06201_00001_mirimage_uncal.fits	M0
jw01517158001_05201_00001_mirimage_uncal.fits'	M1
jw01517164001_03201_00001_mirimage_uncal.fits	M2
jw01517168001_05201_00001_mirimage_uncal.fits	M3
jw01517170001_03201_00001_mirimage_uncal.fits'	M4
jw01517173001_02201_00001_mirimage_uncal.fits	M5
jw01517174001_02201_00001_mirimage_uncal.fits	M6

4.1.1 Cluster Shower

As mentioned above, the term “shower” derives from the most common morphology of the MIRI large events where there is a cluster of classic cosmic rays that are associated with a region of low-level diffuse emission (see Figure 12). This diffuse emission is below the detection threshold (default of 4 - 5 sigma) of the baseline jump detection leading to residuals in the rate images.

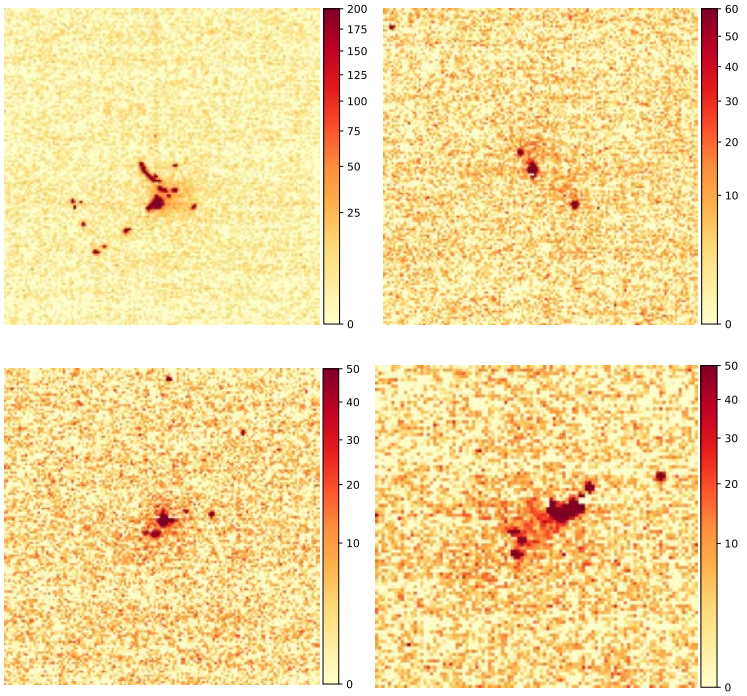

Figure 12 – These are examples of basic MIRI showers. The images are differences between two adjacent groups. In each case, there is a cluster of several classic cosmic rays that is associated with a faint diffuse emission.

4.1.2 Only Faint Extended Emission

As we obtained larger samples and improved our sensitivity, we found that there are several other variations of showers. In Figure 13, we show two difference frames where there is a statistically significant region of diffuse emission without any individual classic cosmic rays. To minimize the effects of these events, a shower detection algorithm needs to be able find and flag this diffuse emission.

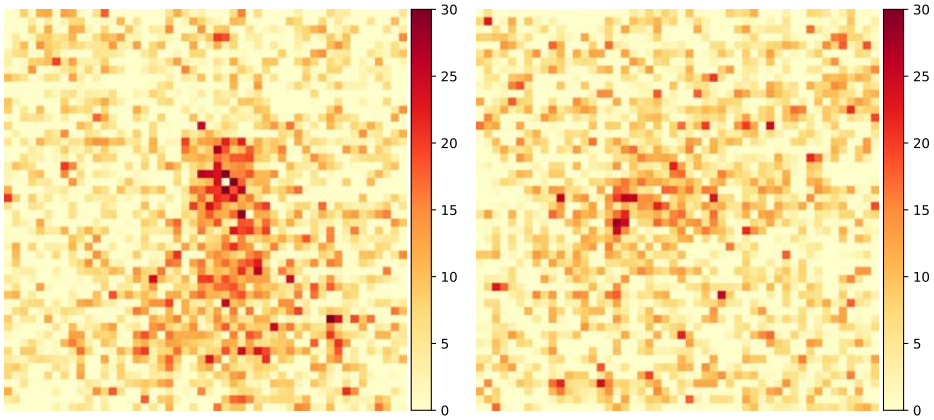

Figure 13 - These difference images show instances of low-level emission that is not associated with any classic cosmic rays. This level of emission is below the detection threshold of the baseline jump algorithm.

4.1.3 Showers that Extend Beyond One Group

Another variety of showers are ones that show extended emission beyond a single group. In Figures 15 and 16, I show examples of two such events. The fact that the extended emission is not limited to one group shows that these events are significantly different from classic cosmic rays. This emission is not limited to just two groups as we will see with the next type of shower.

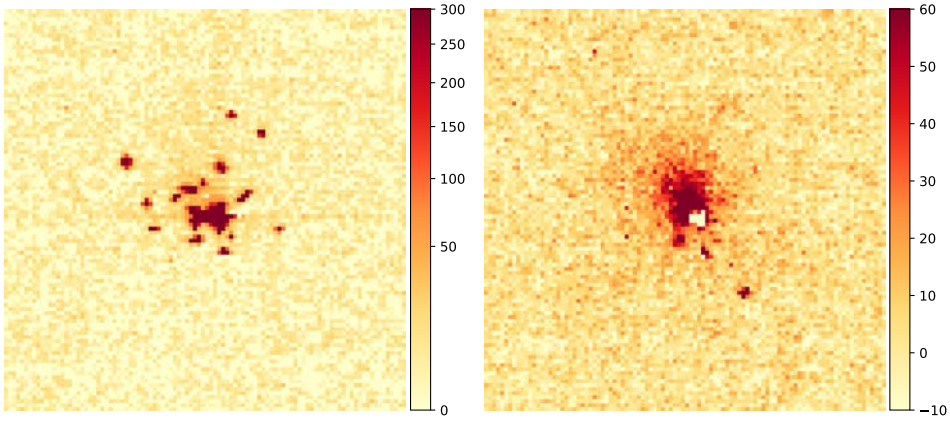

Figure 14 – These are two sequential difference images. Here you can see that there is extended emission in both differences.

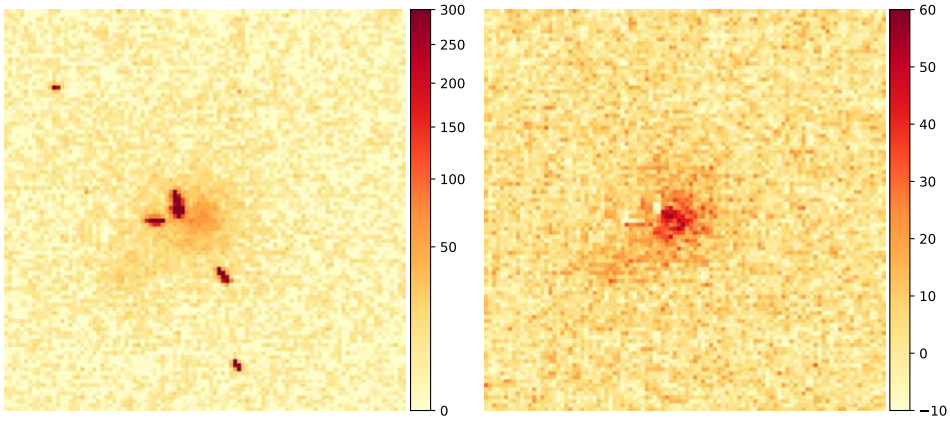

Figure 15 - Another sequence of difference images where the one on the right is for the group after the one on the left. The extended emission on the left is associated with four classic cosmic rays. The difference on the right does not show any classic cosmic rays. Instead, it just shows the same basic morphology of diffuse emission as the first difference.

4.1.4 Comets

The showers that have the largest effect on the rate determination have a morphology that resembles comets. The comets shown in Figure 16 have several common features. The excess of classic cosmic rays is the largest in the first difference. In the second and later differences the nucleus of the comet shows a region of negative differences. Also, the width of the diffuse tail is at a minimum where it joins the nucleus. Finally, the diffuse tail can extend for hundreds of pixels and for a very long time (10's of minutes).

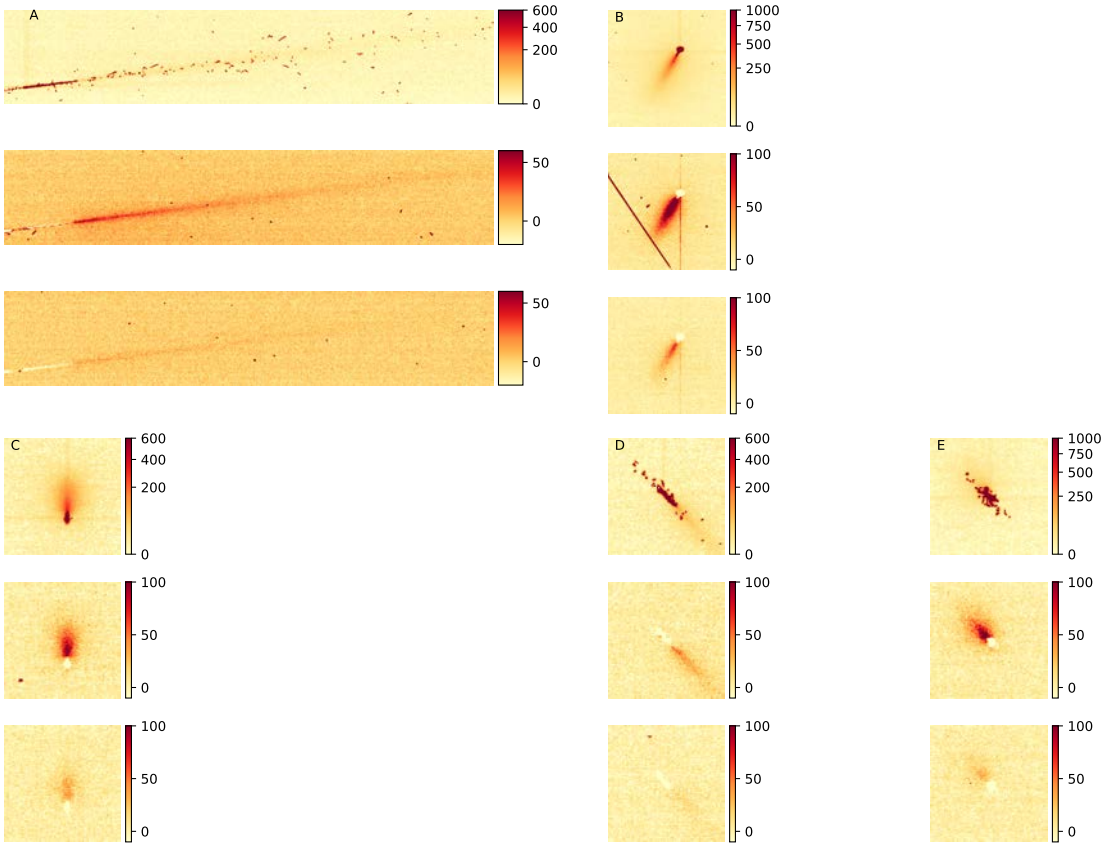

Figure 16 - Examples of Comet events. In each subpanel, the earliest difference is at the top. The difference images are one frame time or 2.77 seconds apart. For each event, I show the first difference where the shower occurs and the two subsequent differences. A) This is the largest event in the set of darks used for this analysis. It extends over 900 pixels across the width of the detector. This is from exposure M1. B) This event is from M5. There is a coincidental classic cosmic ray in the second difference. It is a good example of how classic cosmic rays only affect one difference because there is no sign of the cosmic ray in the last difference. C) From exposure M6. D) From exposure M3. E) From exposure M4.

In Figure 17, I show a higher contrast version of Figure 16A. Here we see that the width of distribution of elongated secondary events increases from left to right. The tails of these secondaries point back to the nucleus of the comet showing that the primary particle arrived from the left-hand side.

Figure 17 - A higher contrast version of the comet shown in Figure 16. The trails of the secondaries point back to the bright steak on the left of the image. This is strong evidence for the triggering particle arriving from the left of the image.

4.2 MIRI Shower Detection

The different morphologies and temporal behaviors between the Near IR snowballs and MIRI showers require different detection algorithms. The key characteristic that is challenging for shower detection is the extended diffuse emission that is not strongly correlated with classic cosmic rays. While basic showers do show an excess of classic cosmic rays that are associated with diffuse emission, the cases where there is only faint extended emission and when the diffuse emission continues for multiple groups are not associated with classic cosmic rays. Therefore, an algorithm to detect faint excess extended emission needed to be developed.

5 Shower Algorithm Description

Like with snowballs, the baseline cosmic ray detection algorithm works correctly for a cluster of classic cosmic rays but is unable to detect and flag diffuse emission below the cutoff threshold (nominally five sigma). This causes the rate solution to include the excess diffuse emission. In the left panel of Figure 18, we see the effect of the unflagged diffuse emission in the rate images. We show a simple example of the problem in Figure 19. Here we see a cluster of classic cosmic rays surrounded by some low-level excess. Figure 20 shows that while the baseline jump detection flags the classic cosmic rays, there is still residual emission.

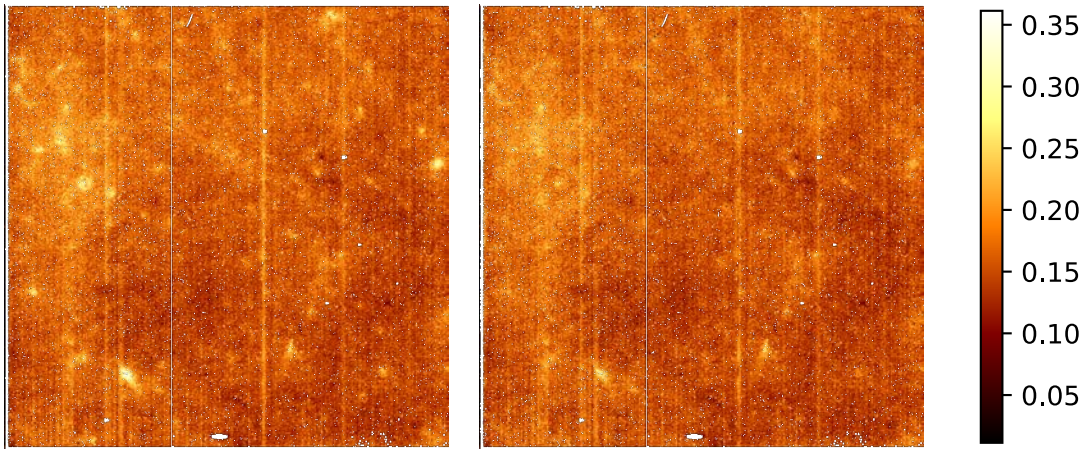

Figure 18 - The no correction (left) and after correction (right) rate images for exposure for a 250-frame MIRI dark. Some residual shower artifacts are still visible.

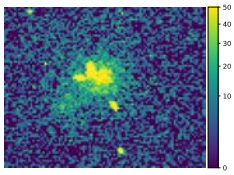

Figure 19 - A single difference of two groups of a MIRI dark. This is a typical shower with several bright pixels and a region of faint emission that surrounds the classic cosmic rays.

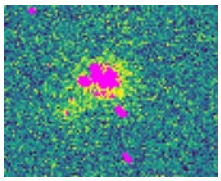

Figure 20 - The difference image shown in Figure 19 with the pixels flagged as Jump by the jump shown in purple. Notice that there is significant unflagged flux.

The first step for the detection of showers is the same as for the detection of classic cosmic rays in that we create a set of differences between groups for each integration. To detect showers, we apply a convolution to each of the difference frames in the integration. The convolution lowers the high frequency noise in the image while maintaining the larger-scale flux. This smoothing allows us to use a significantly lower detection threshold that can detect the relatively faint extended emission of the showers. In Figure 21, we show the default convolution kernel that is used. This is the Ring2DKernal from NumPy. The kernel has two free parameters, the inner and outer radii. We used the Ring2DKernel so that we could exclude any flux from point sources. While we do mask all the pixels that are flagged as Saturated or Jump, there can be residuals that would bias the convolution.

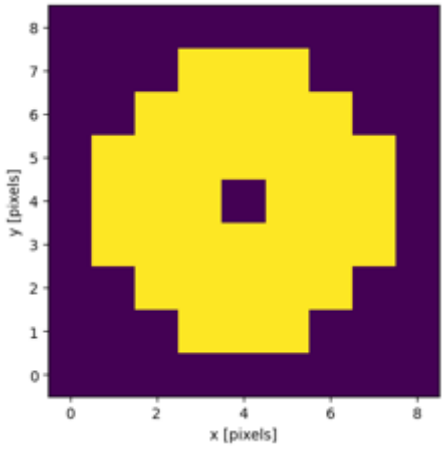

Figure 21 - The default Ring2DKernal used to convolve the masked ratio image to allow the detection of faint extended emission.

Using the default convolution kernel, we are able to detect extended emission that is well below 2-sigma deviations, where sigma is the total noise expectation in the pixel. Besides having a

threshold for the extended emission, the algorithm also requires a minimum area. This decreases the probability of false positives.

Below is a step-by-step walkthrough of the shower detection algorithm.

5.1 The Shower Detection Algorithm for each Integration (performed after the baseline jump detection algorithm)

1. Find the difference of all pixels between groups.
2. Calculate the median difference for all pixels.
3. Estimate the expected sigma of each pixel using the median difference, the read noise, and the detector gain.
4. For each pixel in each group, find the deviation from the median value in units of sigma.
5. For each group
    a. Mask all pixels that are flagged as Jump or Saturated by the baseline jump detection (Figure 22).

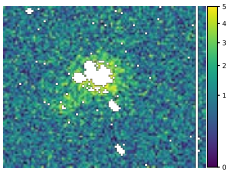

Figure 22 – The difference image with the pixels that are already flagged as either Jump or Saturated are masked (set to white in this image).

    b. Convolve the masked ratio by the kernel (Figure 23).

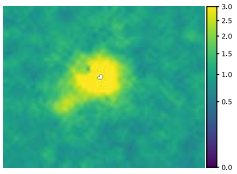

Figure 23 – The resulting image after the convolution has been applied to the masked image. The residual emission is significantly above the background.

    c. Find all pixels in the convolved difference above the **extend_snr_threshold** parameter (Figure 24). This excludes most of the non-diffuse emission.

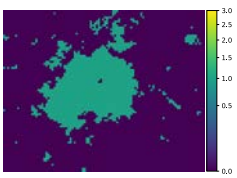

Figure 24 – A binary image showing all pixels that are above the detection threshold. Notice that there are several small clumps of pixels but that the primary area with residual emission forms a continuous region.

d. Find all continuous regions of connected pixels greater than **extend_minimum_area** parameter (Figure 25). By requiring a minimum area, we increase the specificity of the algorithm.

Figure 25 – The region of connected pixels that have a total number of pixels (area) greater than the input parameter.

e. Solve for the minimum enclosing ellipse for every region above the minimum area (Figure 26). We use an ellipse rather than the raw region to smooth out the noise effects. This also captures some low-level extended emission that is below the nominal detection threshold.

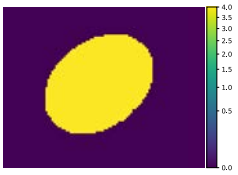

Figure 26 – The smallest ellipse that encloses the region show in Figure 25.

6. For each enclosing ellipse
    a. Extend the ellipse spatially based on the input parameter, **extend_ellipse_expand_ratio**. We expand spatially to flag emission that is below the detection threshold. The default expansion is a factor of 1.2. This is smaller than the snowball expansion because we are already flagging extended emission that is significantly fainter than the classic jump detection.
    7. After all ellipses have been found for all groups, extend the flagging of ellipses to groups after the primary event based on the **time_masked_after_showers** parameter. This is done to deal with the majority of showers that show excess extended emission for a few frames after the primary event. Below I will show that there are still showers that are not fully flagged with this method.

5.2 Shower Flagging Results

The following figures show the results for the first integration for seven dark exposures taken with the CCC closed for at least four hours before the exposure started. Each exposure has two integrations with 250 groups. I focused on the first integration due to the fact that large comet events leave latent images in the second integration. All but one of the large events in these figures are shower events that have occurred in the first integration. (The exception is the upper right residual in M6.)

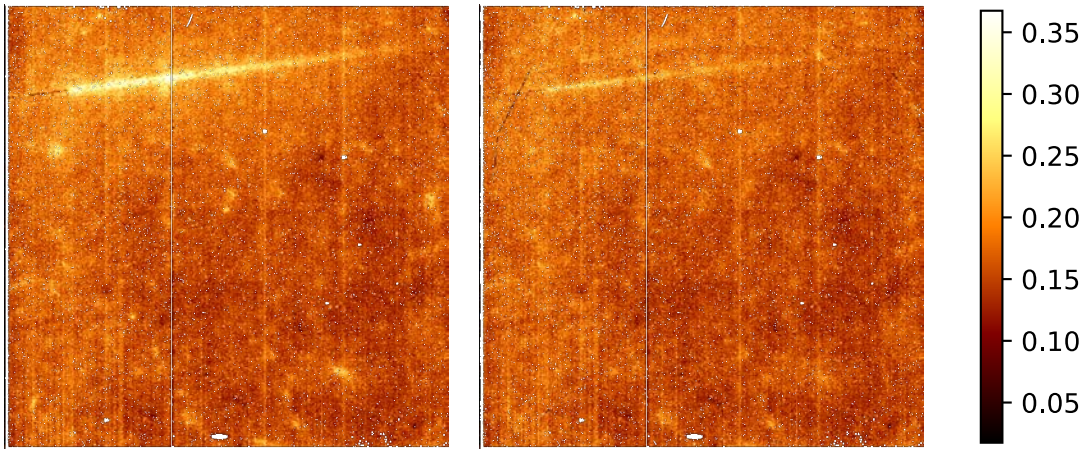

Figure 27 - The before (left) and after (right) rate images for exposure M1.

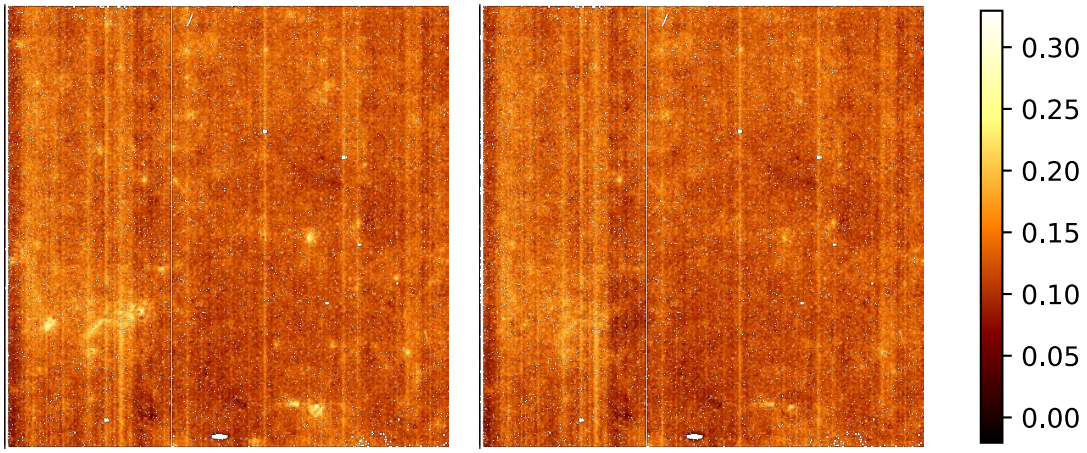

Figure 28 - The before (left) and after (right) rate images for exposure M2.

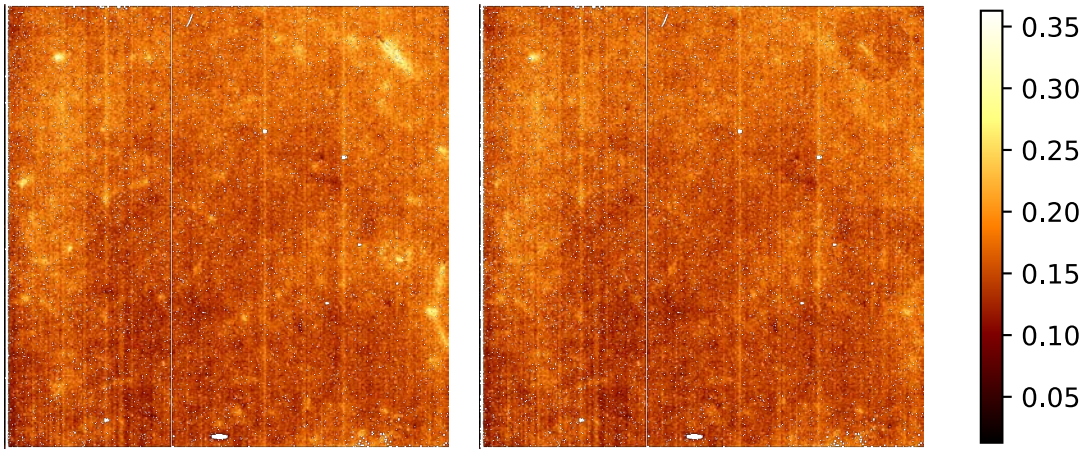

Figure 29 - The before (left) and after (right) rate images for exposure M3.

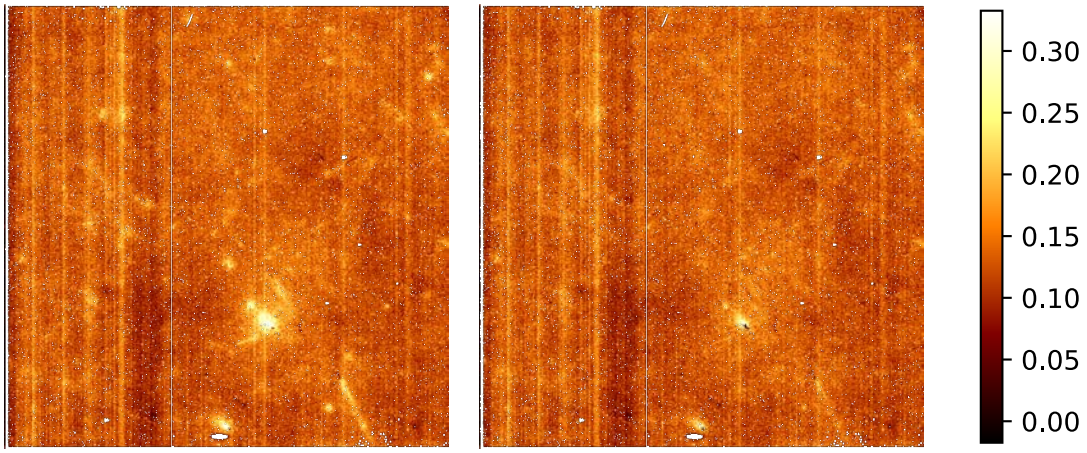

Figure 30 - The before (left) and after (right) rate images for exposure M4.

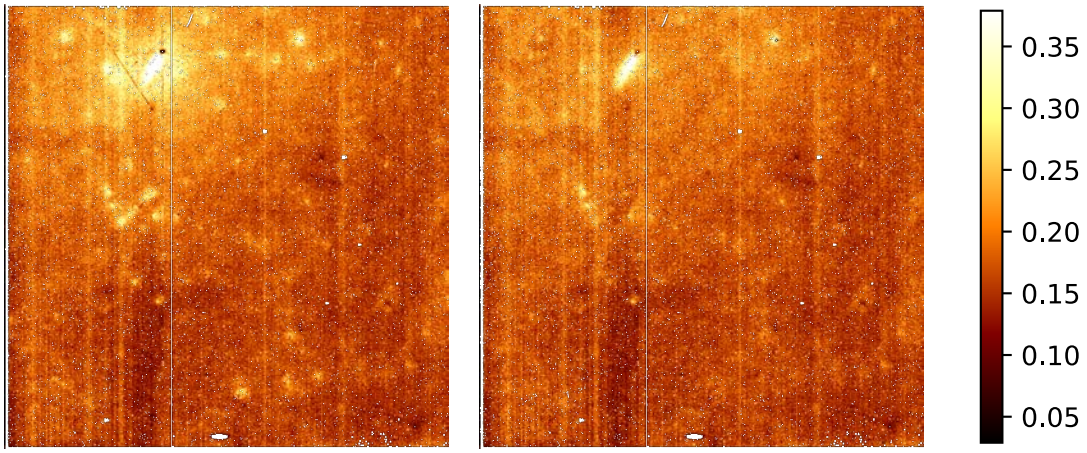

Figure 31 - The before (left) and after (right) rate images for exposure M5.

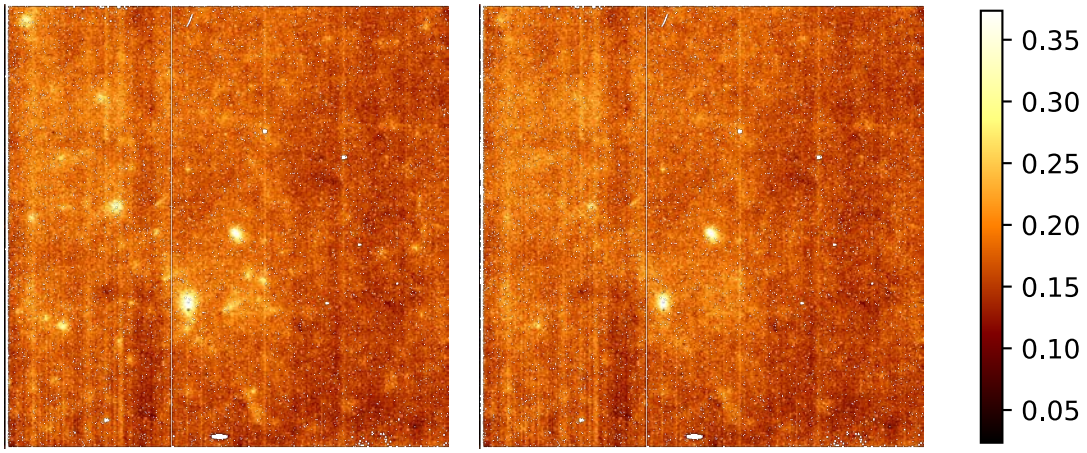

Figure 32 - The before (left) and after (right) rate images for exposure M6. Note that in this integration two of the three major showers are not removed. The upper right residual appears to be a residual from a shower

that occurred relatively close to the start of the integration because it is present in all the differences. The lower left residual is a comet residual that occurred early in the integration leading to a significant residual signal.

As we see in the before and after rate images, while there is significant improvement, there are also significant breakthrough showers. The general pattern of these large breakthroughs is that their morphology would be classified as a comet and that they primarily occur during the first half of the integration. Tests where **time_masked_after_showers** was increased as high as 80 seconds show only small changes in the rate image.
In Figures 34 and 35, I show two plots for the accumulated DN for both integrations in regions with a residual shower. In both cases, the final rate (last 10 groups) is significantly higher than the pre-shower rate. This shows why increasing the number of groups flagged after the shower never yields a correct rate. Charge is coming into the pixel until the end of the integration. In the second integration, we also see that the initial rate is still significantly higher than the initial rate in the first integration. Even the final rate of the second integration is above the initial first frame rate.
Future updates will require that these regions get flagged for all of the remaining integrations in the exposure.

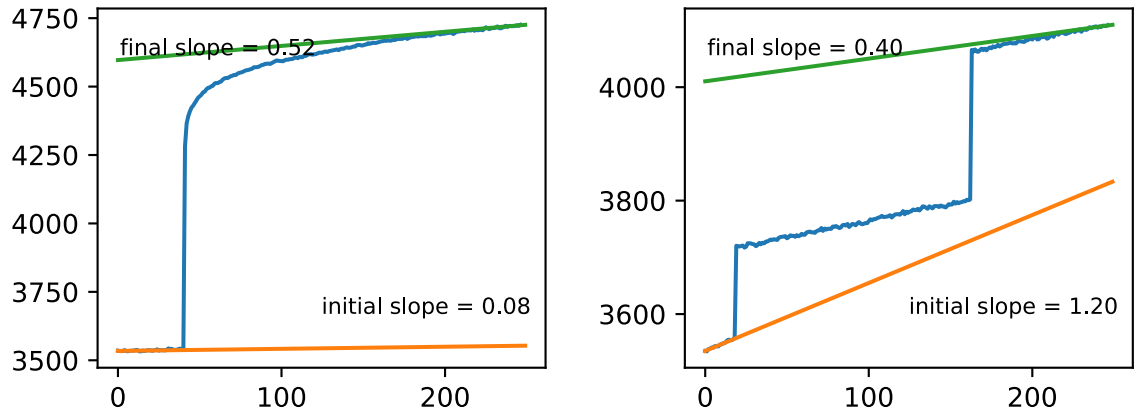

Figure 33 – The two plots show the average accumulated DN values in a 5x5 region in the tail of a comet in exposure M4. This left panel is the first integration, and the right is the second integration. The large jump around group 30 is when the primary event occurred. The orange lines are the rate before the event in integration 1 and the rate of the first 10 groups in integration 2. The green lines are the rate of the last 10 groups of each integration.

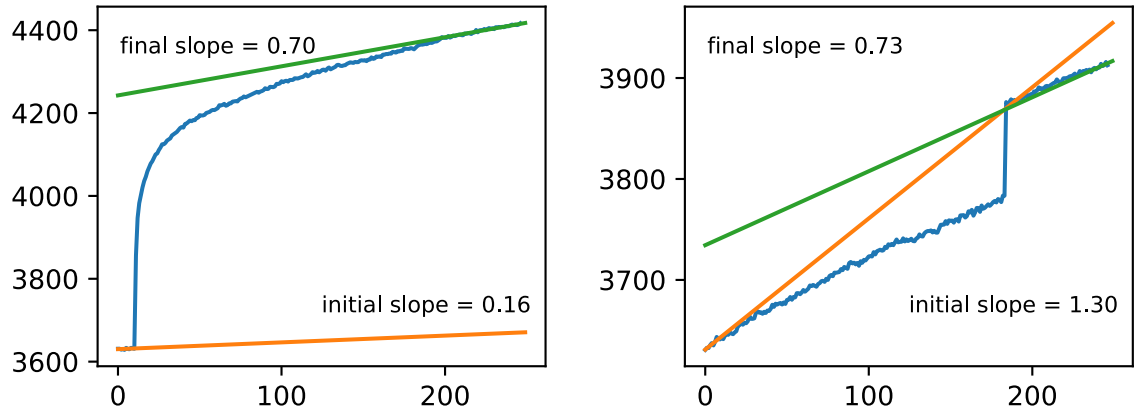

Figure 34- The two plots show the average accumulated DN values in a 5x5 region in the tail of a comet in exposure M6. The left panel is the first integration, and the right is the second integration. The large jump around group 12 is when the primary event occurred. The orange lines are the rate before the event in integration 1 and the rate of the first 10 groups in integration 2. The green lines are the rate of the last 10 groups of each integration. Note that the jump in the second integration around group 180 is a classic cosmic ray that affects the average.

5.3 Outstanding issues with Shower detection

- Comet events that cause very long-term diffuse emission need to be identified and flagged for the duration of the exposure.
- Some MIRI observing modes have calibration issues that cause the early groups in an integration to have systematically high count-rates compared to the median rate. This is misidentified by the shower algorithm as a very large shower. Until the calibration issues are addressed, these modes cannot use shower detection.
- Most of the MIRI subarrays have a 390 Hz EMI noise component. This correlated noise means that, after the convolution is performed, the noise level is significantly elevated. There is an ongoing enhancement to the production pipeline to implement a new step to remove the 390 Hz noise component. In testing with the prototype code, we have seen almost all of the 390 Hz noise removed. Until the 390 Hz is removed from the MIRI subarrays with 390 Hz noise, shower detection should not be used for those subarrays.

5.4 Jump Step Parameters that control the Shower Detection and Flagging

The following is a list of the parameters that affect shower detection and a short description of what the parameter controls. For each parameter the value in parentheses is the default value in the code. This can be overridden by either a parameter reference file or a command line parameter.

- Find_showers – This is a Boolean value that needs to be True for the shower detection algorithm to run. This should only be set to True for MIRI observations. (False)
- Find_extended_emission – This is a Boolean value that needs to be False to turn off the near infrared snowball algorithm. This should always be False for MIRI (False)

- Extend_snr_threshold – This is the detection threshold that is used on the convolved masked ratio. If there are too many false positive detections, increasing this value will reduce the number of false positives. This may need to be higher for subarrays with 390 Hz after the EMI correction is applied. (1.2)
- Extend_min_area – This is the minimum area of regions above the SNR threshold required for a region to be detected as a shower. If there are small regions of non-detected extended emission, lowering this value would allow them to be detected. (90)
- Extend_inner_radius – The inner radius of the ring2Dkernal that is used in the convolution of the masked ratio. (1)
- Extend_outer_radius – The outer radius of the ring2Dkernel that is used in the convolution of the masked ratio. If there is faint extended emission that after convolution is not detected, increasing the outer radius would lower the random noise and allow this fainter emission to be detected. Increasing the radius does increase the size of the convolved region. To avoid flagging too many pixels the extend_ellipse_expand_ratio could be decreased. (2.6)
- Extend_ellipse_expand_ratio – The relative increase in the size of the detected extended emission ellipse. This value could be reduced to decrease the number of pixels flagged for each detected region of extended emission. (1.1)
- Time_masked_after_showers – The time in seconds after a shower where all pixels that are flagged as Jump in the original shower are also flagged as Jump. There are rare cases of showers creating regions of extended emission that last longer than the default time. By increasing this time, those regions could be flagged as Jump and not affect the final rate calculation. (15)
- max_extended_radius - This is set to 200 pixels to prevent rare outlier values from flagging all the pixels and crashing the production pipeline. If a large snowball seems to have the core correctly flagged but there is a residual ring of halo emission, changing this parameter to a much larger number (> 500) can improve the results. (200)

6 Analysis

In Figures 36 and 37, I show the sizes and ellipticities from a set of NIRSpec and MIRI darks. The figures show that the relative size distributions are similar but that the overall size of showers is about a factor of two larger than snowballs. The difference in the ellipticity distributions is striking. The snowballs have a large fraction of completely circular events with a small fraction of highly elliptical events. In contrast, the showers are only rarely circular with the most common morphology being quite elliptical.

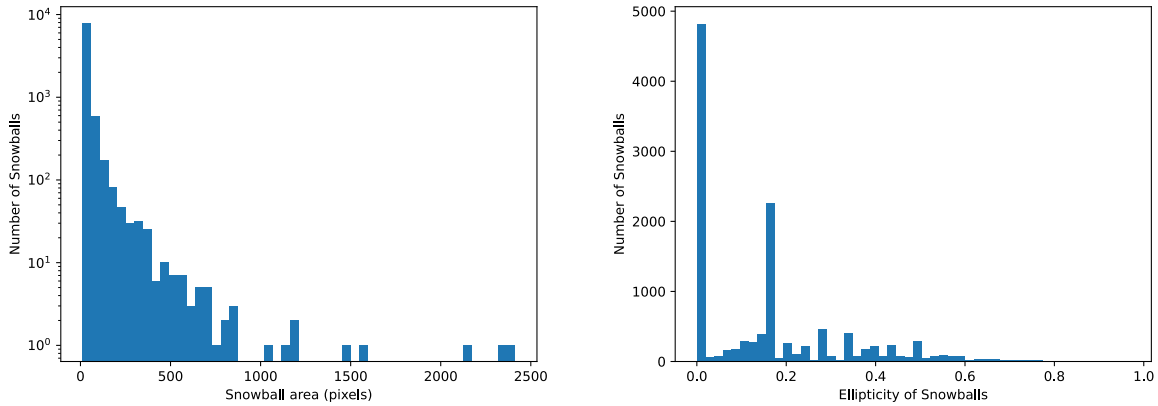

Figure 35 - (Left) The distribution of snowball sizes from four 1-hour NIRSpec darks. (right) The distribution of the ellipticities of the snowballs.

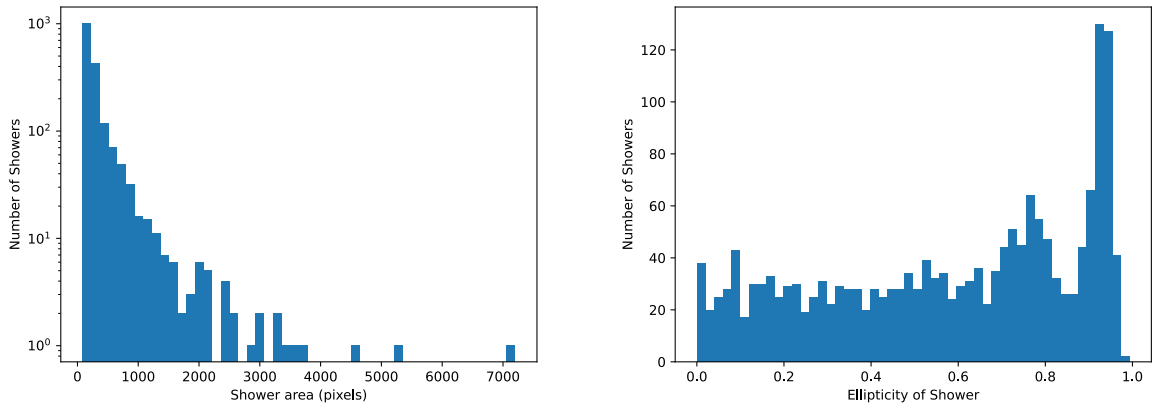

Figure 36- (Left) The distribution of shower sizes from seven 23-minute MIRI darks. (right) The distribution of the ellipticities of the showers.

The differences in the distributions of the two types of events are consistent with the differences in the images I have shown above. Clearly, these two types of events have significantly different triggering mechanisms.

The high ellipticity of the MIRI showers combined with the usual association of a cluster of classic cosmic rays that appear to be secondary events (see Figure 17) implies that showers are triggered by the interaction of a particle with something in the detector. The fact that the locations of these secondaries are within 10's of microns implies that they have only traveled a few hundred microns at most from the primary interaction. One explanation of the comet events (Figure 16) could be they are caused when the interaction occurs very close to but outside of the depletion region, allowing a large fraction of the energy to trigger carriers that can easily travel to the depletion region over a period of time.

The overall high ellipticity of the showers is probably associated with the relatively large thickness of the detector layer compared to the near infrared detectors. This greatly increases the

probability of higher angles of incidence. This also implies that the particles can travel through a significant number of pixels.
The mostly circular snowballs suggest that the incoming particle interacts with the HgCdTe very close to the surface of the detector and that all of the energy is deposited at once. Snowballs rarely have associated classic cosmic rays. This implies that the snowballs are caused by the primary particle. An additional difference is that the NIR HgCdTe material has a larger mass that the Silicon that dominates in the MIRI detector (˜150 g/mol vs 28 g/mol).

7 References

Hilbert, B. 2009, "Snowballs" in the WFC3-IR Channel: Characterization. WFC3 ISR 2009-43. https://www.stsci.edu/files/live/sites/www/files/home/hst/instrumentation/wfc3/documentation/instrument-science-reports-isrs/_documents/2009/WFC3-2009-43.pdf Dec 2009.

McCollough, P. 2009, Radioactivity in HgCdTe devices: potential source of "snowballs", WFC3 ISR 2009-44. https://www.stsci.edu/hst/wfc3/documents/ISRs/WFC3-2009-44.pdf

Rauscher et al. 2014, PASP, 192, 942, 739, https://dx.doi.org/10.1086/677681